

# The VLITE Commensal Sky Survey (VCSS) Epoch 1 Bright Catalog Release

WENDY PETERS <sup>1</sup> TRACY CLARKE <sup>1</sup> SIMONA GIACINTUCCI <sup>1</sup>  
KRISTINA NYLAND <sup>1</sup> AND EMIL POLISENSKY <sup>1</sup>

<sup>1</sup>*Code 7213, Naval Research Laboratory  
4555 Overlook Ave SW,  
Washington, DC 20375, USA*

## ABSTRACT

This document describes the first data release of the VLITE Commensal Sky Survey Epoch 1 (VCSS1). This 340 MHz survey was observed simultaneously with Epoch 1 of the 3 GHz VLA Sky Survey (VLASS). The data for VCSS1 come from the VLA Low-band Ionosphere and Transient Experiment (VLITE), and all data products reported here are produced by the Naval Research Laboratory (NRL). The catalog consists of components determined by PyBDSF fitting on individual mosaic images where the fitted synthesized beams range from  $1.0''$  (minor axis) to  $3.0''$  (major axis). Details of the instrument, observing mode, processing and data products are provided in this memo. This first data release comprises only the bright ( $> 50\sigma$ ) sources due to significant bias in flux for weaker sources as described in the document. We detail a number of known limitations on the catalog, including the need to add a 15% flux scale uncertainty to cataloged errors, and we adopt a positional uncertainty of  $2''$  for the catalog. The noise is not uniform across the sky for VCSS1, but the average  $1\sigma$  noise is  $\sim 3$  mJy/bm<sup>-1</sup>. We estimate that the  $50\sigma$  catalog is complete at  $> 50\%$  for sources with peak brightnesses above 200 mJy/bm or integrated fluxes above 300 mJy.

## 1. OVERVIEW

A summary of the basic observational parameters for the VCSS Epoch 1 bright catalog release is given in Table 1. The angular resolution typically ranges from  $10''$  (minor axis) to  $30''$  (major axis) and varies considerably across the sky; however it is on average equivalent to the area of a  $15''$  round beam. We assume typical VLA snapshot sensitivity to extended sources in estimating the largest angular size (LAS). The sensitivity varies considerably across the sky as detailed below. The catalog covers most of the sky above dec  $-40^\circ$ , but there are gaps due to failed

Central Frequency	340 MHz
Bandwidth	33.6 MHz
Angular Resolution	$\sim 15''$
LAS	8.5
Average sensitivity ( $1\sigma$ )	3 mJy $\text{bm}^{-1}$
Sky Coverage	30,000 $\text{deg}^2$
Sources	52,844

**Table 1.** VCSS Epoch 1 Bright Catalog summary

observations (see Figure 1). The IAU naming convention for the sources is VCSS1 JHHMMSS.s+DDMMSS <sup>1</sup>.

## 2. INTRODUCTION

The initial development of sub-GHz feeds on the National Radio Astronomy Observatory (NRAO) Very Large Array (VLA) in the 1980’s and 1990’s led to receivers operating at 330 and 74 MegaHertz (MHz). Together with new methodologies for correcting for ionospheric fluctuations, these systems opened up the HF/VHF frequency window to high resolution interferometric studies and spurred multiple generations of new low frequency instrumentation and science across the globe. In 2013, the U.S. Naval Research Laboratory (NRL) worked with the NRAO to enable a new commensal operation mode for the 330 MHz feeds that allows them to collect data during nearly all regular VLA operations.

The VLA Low-band Ionosphere and Transient Experiment (VLITE) started taking data on 2014-11-21 and has recorded roughly 6200 hours of data each year since that time. The system has now been running for 7.5 years and is expected to continue recording data for the foreseeable future. Data are recorded on up to 18 VLITE antennas, correlated, and transferred to the NRL for automated pipeline processing and archiving. The instrument records roughly 22 Terabytes (TB) per year of raw data and the processing generates a similar volume of data products.

In the summer of 2016, during initial testing for the VLA Sky Survey (VLASS), a special correlator mode was enabled and tested on VLITE to allow the processing of on-the-fly (OTF) data. VLASS observes by scanning in right ascension (RA) along lines of constant declination which are spaced by  $7'.2$ . VLITE data are allowed to accumulate using a standard 2 second sampling, as the antennas move through an angular distance of  $1.5^\circ$ . At the standard slew rates of the VLASS, this corresponds to  $\sim 28$  seconds of time over most of the sky. These data are then correlated, using the midpoint of the motion as the phase center. The result is short “snapshots” that have a smeared or elongated primary beam response. We image each snapshot at

<sup>1</sup> <http://cds.u-strasbg.fr/cgi-bin/Dic?VCSS1>

the phase center. The choice of  $1.5^\circ$  allows for sufficient data to reliably image the snapshot, and is comparable to the  $1.25^\circ$  half power point of the un-smearred primary beam response of the instrument.

### 3. DATA AND REDUCTION

We refer to all data collected during VLASS (Lacy et al. 2020) as the VLITE Commensal Sky Survey, or VCSS. Following the conventions of VLASS, Epoch 1 is referred to as VCSS1, and includes observations from September 2017 to February 2018, and March to July 2019.

VLASS divides the sky into a series of tiles for observing, each roughly  $10^\circ \times 4^\circ$ . Observations are scheduled in a patchwork fashion and adjacent tiles may be observed on different days, months, or even years of a given epoch. Because the VLITE field of view is considerably larger (FWHM  $2.5^\circ$ ), than the 3 GHz field of view (FWHM  $14'$ ), there is a great deal of overlap between observations towards the edge of each tile. This means that our final mosaic images include snapshots from multiple dates in most positions on the sky. As a result, the distinction drawn by VLASS between Epoch 1.1 and Epoch 1.2 is not generally relevant for VCSS1 mosaics.

### 4. PROCESSING

VLASS scheduling blocks typically include one or two primary calibrator scans (either 3C286 or 3C138) each day, and phase calibrators throughout the observations. The 3 GHz phase calibrators are not always suitable for use at 340 MHz, and are not necessary for reliable imaging. For this reason, they are excluded from VCSS1 data reduction. Using a dedicated processing pipeline which combines Python code with standard Orbit and AIPS tasks, VCSS1 observations for a given day are combined, and the primary calibrator scans are used to derive complex gain and bandpass solutions. The data are flagged, and then phase calibrated using a global sky model based on the NRAO VLA Sky Survey (NVSS: Condon et al. 1998).

Each snapshot is individually imaged. Snapshots with less than 20 seconds of data and/or fewer than 1300 visibilities (after flagging and primary calibration) are not imaged due to poor image fidelity. This typically, although not entirely, excludes data recorded as the antennas move from one declination strip to the next. It also means that even when VLITE is functioning during a given observation, if enough antennas are not working for any reason, then the final data cannot be imaged.

### 5. MOSAICS

The initial processing of VCSS Epoch 1 included more than 170,000 snapshots, of which roughly 135,000 passed our quality checks. These snapshot images are corrected for the smearred primary beam response, and then combined into a final mosaic image using additional software in Python and Orbit.

#### 5.1. *Primary Beam Response*

The primary beam response is assumed to be similar to that of the standard VLITE response during 3 GHz observations, but “smeared out” in the direction of the telescope movement.

Early processing of the snapshot data led to the discovery of a small,  $6'$  pointing offset between the 3 GHz and 340 MHz receivers. This is a result of the geometry of the VLA antennas with the 340 MHz receivers at the prime focus, and the GHz receivers in a ring at the Cassegrain focus position. The antennas have an alt-az mount, so the angle between the prime focus and 3 GHz receivers varies with parallactic angle. As a result, the precise pointing offset “wanders” and must be calculated for each individual observation. The offset is small enough that the errors introduced by ignoring it are trivial ( $\ll 1\%$ ) near the pointing center, but may be quite large (10%) at the FWHP radius. They must be corrected in order to accurately measure flux across the entire field of view. In addition, the 340 MHz system on the VLA has a known primary beam asymmetry. We have modeled this asymmetry using VLITE C-configuration data and the WENSS catalog (Rengelink et al. 1997).

Our final beam models include the pointing error and the asymmetry, and are calculated for each snapshot by summing the response at each 2 second integration present in the final image, and then normalizing by the number of integration steps. The result is an offset, smeared and slightly asymmetric response. Testing of the effect of these corrections on bright sources observed in many snapshots at a variety of radii show that the result is accurate to well within the uncertainties of the flux scale.

## 5.2. Sky Coverage, Resolution and Sensitivity

In Figure 1, we show the area on the sky covered by the mosaics in VCSS1. The coverage holes correspond to tiles for which VLITE either was offline completely, or had data that was insufficient for imaging (typically due to a lack of antennas), or are in areas of the sky where bright sources in the beam sidelobes (e.g. near Cygnus A) destabilize the imaging.

We made the choice, early in the processing, to image each tile with a “best fit” beam for that tile. At the time, we did not fully understand the degree of overlap between tiles observed on different days, nor the degree to which the beams would vary from one day to the next. In practice the beams can be at any angle and vary in major axis from  $12''$  to  $30''$ . The average beam area is equivalent to that of a  $15''$  round beam, and we thus quote that as the “standard” resolution. The images were not convolved to a common resolution before combining them into mosaics. As a result, any given position in the mosaics may include images with differing beams, and the resulting “RMS noise” is highly non-Gaussian. However, the nominal RMS  $1\sigma$  sensitivity is about  $3 \text{ mJy } \text{bm}^{-1}$  over most of the sky.

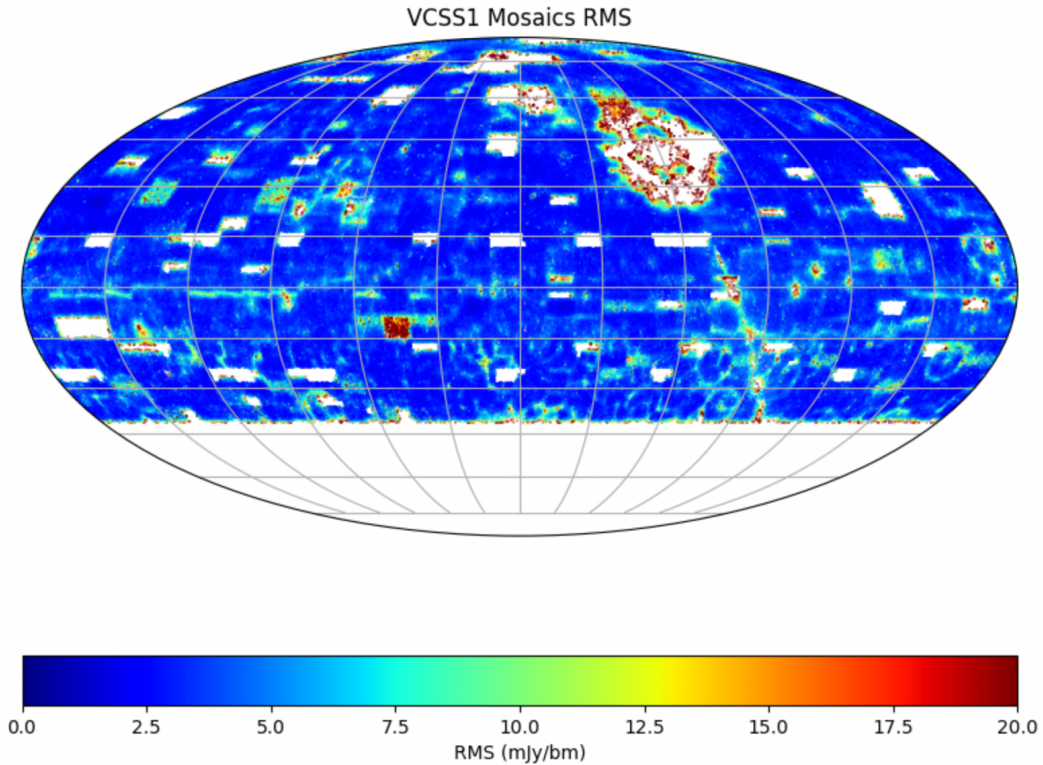


**Figure 1.** An image showing the VCSS1 mosaic coverage, with colors corresponding to local RMS values near cataloged sources. The average  $1\sigma$  noise is  $3 \text{ mJy bm}^{-1}$ . The small higher-noise tiles (e.g. at  $\text{RA} \sim 3 \text{ hrs}$ ,  $\text{Dec} \sim -12^\circ$ ) are likely the result of gain errors in the primary calibration. The Galactic Plane is clearly visible, as are areas of increased noise when sources such as Cygnus A and Cas A are in the primary beam sidelobes.

## 6. THE CATALOG

Each VLITE mosaic image is searched for sources using dedicated Python software which runs the Python Blob Detector and Source Finder (PyBDSF, [Mohan & Rafferty 2015](#)). Each image is decomposed into a set of islands containing emission from astrophysical sources and then each island is fit with Gaussian components to extract source properties such as position, size, flux, source complexity, etc.

### 6.1. Flux Scale

The mosaics from VCSS1 are created by combining multiple overlapping but offset snapshot images at each sky position. We assume that the overall flux reliability of any given snapshot is roughly 15% consistent with that found in regular VLITE operations. We use the [Perley & Butler \(2017\)](#) fluxes for 3C138 and 3C286 to set the primary flux scale.

The process of combining the snapshots into a mosaic introduces a pronounced bias in the final source fluxes. The reasons for this are not fully understood; similar

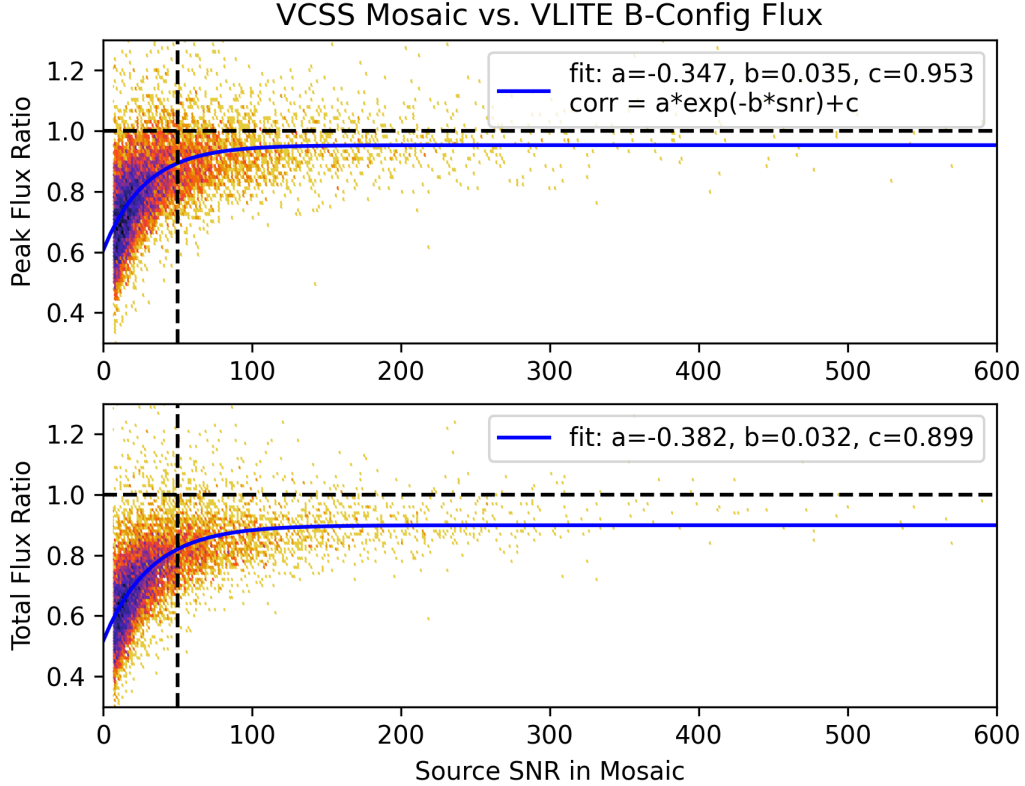


**Figure 2.** The ratio of VCSS1 mosaic fluxes to VLITE archival fluxes, plotted as a function of the source SNR. To make the fit as robust as possible, we have restricted to isolated point sources which are detected at greater than  $8\sigma$  in both catalogs.

combinations of standard VLITE data do not show any evidence of this bias, which suggests that it is not a software or beam issue. Likewise, the smeared primary beam we use to correct the data appears to reliably correct the snapshots themselves without introducing any error. While some of the effect may be due to small positional shifts between each snapshot, efforts to correct snapshots for an average positional shift before combination have proven ineffective at ameliorating the bias. It may simply be that the smeared snapshot response leads to noise that is so severely non-Gaussian that it has unpredictable effects when the images are combined. While we cannot fully explain the resulting bias, we have made every effort to characterize it by comparing to un-biased measurements.

We select a sample of isolated point sources fit as single component Gaussians ( $S\_Code = 'S'$ , see Appendix A) in the VCSS1 mosaics, which have no other sources within  $1'$ , a  $SNR > 8$ , and fitted total and peak fluxes within 10% of each other. We matched these to entries in the VLITE archive using a  $5''$  radius. To avoid resolution complications, we included only VLITE measurements in the B and BnA configurations. When more than one measurement of a source is present in the VLITE archive, we further require that it always be fit as a single component, and that its

Type	a	b	c
Peak	-0.347	0.035	0.953
Total	-0.382	0.032	0.899

**Table 2.** Coefficients to use when correcting VCSS1 sources for flux bias.

variability between measurements at different times is less than 25%, and use median flux and SNR values. As with the VCSS1 sources, we restrict to compact sources which are brighter than  $8\sigma$ . The final matched sample includes 20,949 sources.

In Figure 2, we plot the ratio of the VCSS1 mosaic fluxes to VLITE B and BnA configuration archival fluxes for the matched sample as a function of the source SNR. We have fit the peak and total flux data to an exponential curve of the form:

$$corr = a \times e^{-b \times SNR} + c \quad (1)$$

The coefficients  $a$ ,  $b$ , and  $c$ , which can be used to correct any source in the catalog, are given in Table 2. Uncorrected fluxes should be divided by this correction factor to adjust for the bias. This correction has been applied in the catalog “corrected flux” columns. We assume the bias calculated from the point sources will also be correct for the sources fit as multiple or complex by PyBDSF.

The bright catalog lower limit of  $50\sigma$  was chosen to restrict the bias to be comparable to the assumed 15% flux reliability for all catalog sources. The final bias is  $\sim 5\%$  and  $\sim 10\%$  for the peak and total fluxes, respectively, of the brightest sources, and  $\sim 11\%$  and  $\sim 18\%$  for the faintest sources in the bright catalog.

## 6.2. Positional Accuracy

In order to investigate the positional accuracy of the catalog, we match a sample of 20,900 isolated point sources from the  $50\sigma$  sample to the TGSS-ADR1 (Intema et al. 2017) catalog using a  $10''$  matching radius. The average offset in RA is  $-0.''09$  and in Declination it is  $0.''4$ . The combined accuracy in the comparison is about  $1.5''$ , comparable to the  $2''$  accuracy of the TGSS-ADR1 survey itself.

We note that there are some areas on the sky where the offsets are much greater than average. Most of these are due to a very poor NVSS sky model (e.g. in the Galactic Plane area) or to a known offset between the peak flux position of a bright source at 1.4 GHz and 340 MHz (e.g. near 3C273). In general, if positional accuracy is a concern, it is best to check neighboring sources to derive the local accuracy and/or corrections.

In Figure 3, we plot the Declination of each source vs its RA and Declination offsets for the  $50\sigma$  sample. While the RA plot suggests that the offsets are uncorrelated with the Declination, there is a clear trend in the Declination offsets. This is analogous to

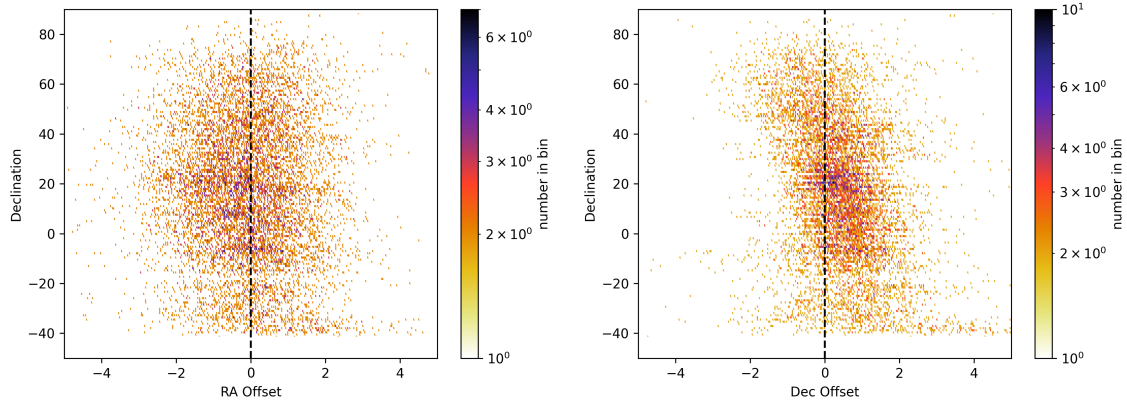


**Figure 3.** The RA offset (left) and Declination offsets (right) of VCSS1 sources in the  $50\sigma$  catalog as a function of Declination.

the known astrometric errors reported in declination for VLASS epoch 1 quick-look images (VLASS Memo #14<sup>2</sup>), and is a well-understood error of imaging snapshots without proper 3D projection. As described in that memo and in Section 4.3 of Condon et al. (1998), hour-angle dependent corrections to the directional cosines can be used to fix the problem in the snapshots; however they cannot be applied to the mosaic images, which combine snapshots over a wide range of hour angles. Except at the very lowest declination, the errors are within the range  $\pm 2''$ , which is only slightly larger than our estimate of the average positional accuracy. We thus adopt  $2''$  as the final accuracy of this catalog.

To further investigate any systematic positional errors, we matched the VCSS1 catalog to sources in the Gaia Early Data Release 3 (Gaia Collaboration et al. 2021). The resulting positional errors on VCSS1 sources increase within  $30^\circ$  of the Galactic Plane, as seen in Figure 4. An unexpected result is the apparent small offsets near the Galactic Center; it is possible this is simply a result of chance superposition in this extremely crowded region of the sky.

### 6.3. Point Source Metric

Determining whether sources are compact or extended (unresolved or resolved) is complicated by inherent biases in source finding algorithms. Source finders like PyBDSF fit 2D elliptical Gaussians to intensity peaks within islands of pixels above a given threshold. Noise pixels statistically above the threshold are included around the island perimeter and bias the fitted Gaussian wider than the true source size (Hales et al. 2012; Hopkins et al. 2015). Weaker sources with peaks closer to the noise floor

<sup>2</sup> [https://library.nrao.edu/public/memos/vla/vlass/VLASS\\_014.pdf](https://library.nrao.edu/public/memos/vla/vlass/VLASS_014.pdf)

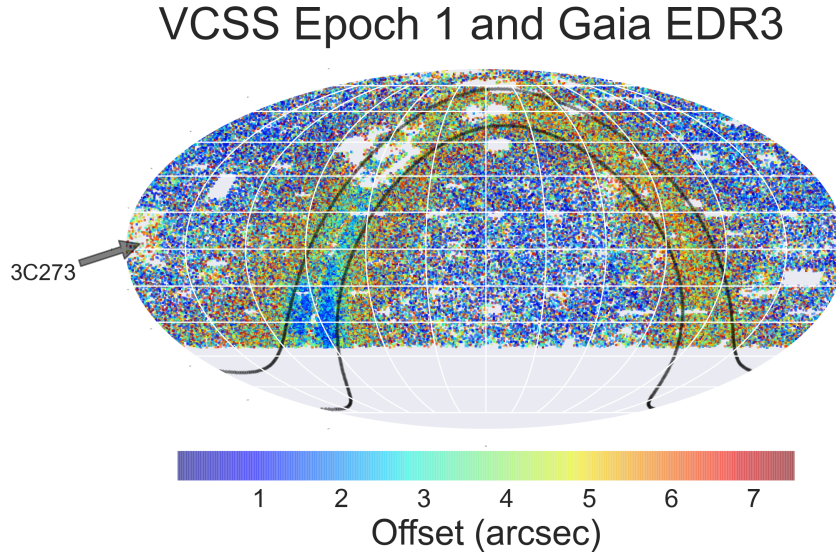


**Figure 4.** A skymap (RA, DEC) of the offsets between VCSS1 and Gaia EDR3 showing the generally good agreement away from the Galactic Plane and 3C273. The black lines indicate the location of the Galactic plane and are drawn at  $\pm 10^\circ$  in Galactic longitude.

are affected more than stronger sources. This bias complicates the use of deconvolved sizes as a metric of source compactness.

An approach that accounts for these effects uses the source total to peak flux ratio,  $R = S_t/S_p$ , of single component sources (S\_Code = ‘S’, see Appendix A) binned by SNR. Extended sources are removed by calculating the average and standard deviation of  $R$  in each bin after iteratively removing  $2\sigma$  outliers. The  $+2\sigma$  envelope is then fit with an empirical equation smoothly varying with SNR (e.g. Eqn. 3 in [Intema et al. 2017](#)). A source compactness metric is defined as:  $R_{2\sigma}/R$ , where  $R_{2\sigma}$  is the flux ratio given by the fitted equation. Compactness defined this way is a statistical metric. Single component sources with compactness  $> 1$  have a  $\sim 97\%$  chance of being unresolved.

Applying this method to the mosaics catalog sources is complicated by the combination of snapshots with restoring beams of different sizes and orientations used to make the mosaics. The uncertainty in the adopted restoring beam adds another component of uncertainty to source flux ratios. Rather than attempt to account for this, we instead apply the approach above to the snapshot source catalog and give the median snapshot compactness of each  $50\sigma$  catalog source.

#### 6.4. *Completeness*

Noise variations across the survey footprint create a brightness-dependent incompleteness in the VCSS1  $> 50\sigma$  catalog. Additional sources are missed that have sufficient integrated flux, but are extended over large solid angles such that their peak brightnesses fall below the selection threshold.

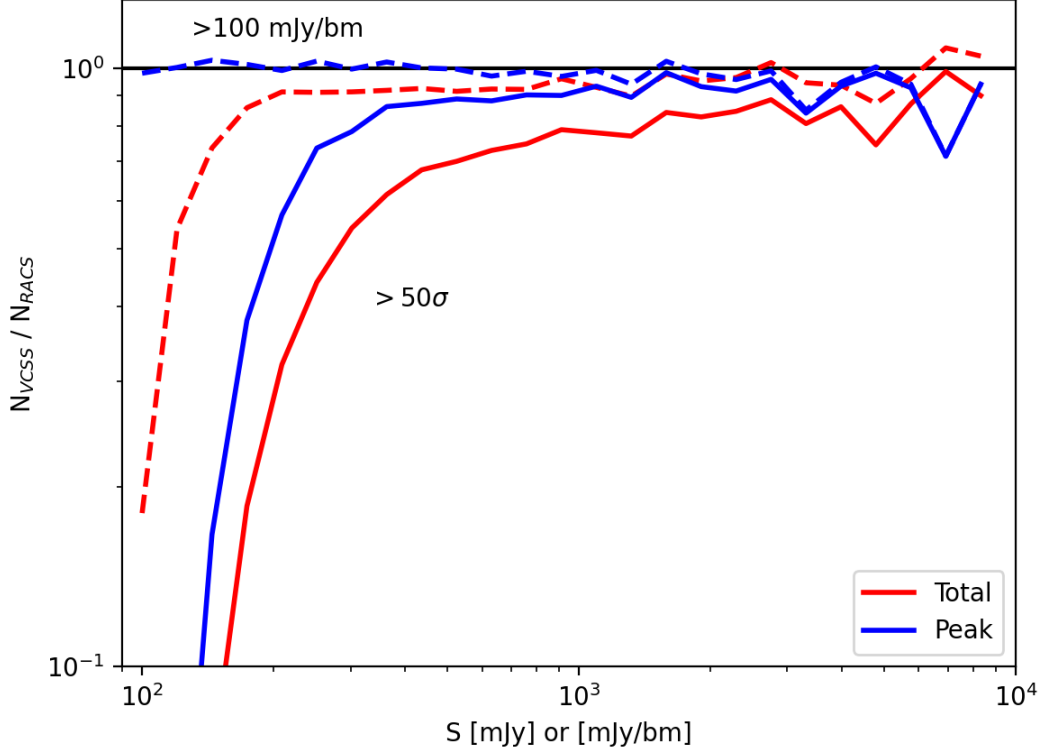


**Figure 5.** Completeness estimates for VCSS1. Dashed lines show the source counts for a sample above a fixed brightness ( $> 100$  mJy/bm), while solid lines show the bright sources above a fixed SNR ( $> 50\sigma$ ). The counts in each flux bin are normalized by the source counts from the RACS catalog scaled to 340 MHz.

To estimate the fraction of sources correctly identified we use the Rapid ASKAP Continuum Survey (RACS; Hale et al. 2021) to model the source distribution. RACS is a 887.5 MHz survey with similar resolution and sky coverage that partially overlaps VCSS1, but contains about four times more sources due to greater sensitivity. RACS fluxes are scaled to VLITE’s frequency using the median spectral index of more than 26,000 point sources matched to single component VCSS1 sources with fluxes  $> 20\sigma$ . Peak and total fluxes are scaled separately with  $\alpha = -0.685$  and  $-0.751$ , respectively, where  $S \propto \nu^\alpha$ . Sources are binned by flux with the bin counts normalized by the survey area. We use a HEALPix (Górski et al. 2005) tiling of the sky and sum pixels containing sources to estimate the RACS sky coverage as 28,000 deg<sup>2</sup>, and VCSS1 as 30,000 deg<sup>2</sup>.

Figure 5 shows the VCSS1 to RACS count ratios for the  $50\sigma$  catalog and a sample above a fixed brightness of  $> 100$  mJy/bm. The fixed brightness sample is unaffected by noise variations with ratios near unity for all brightness values, indicating this sample is complete and the scaled RACS catalog is a good model for the source distribution at 340 MHz. Incompleteness in the total flux counts near the brightness

cut is due to extended sources. The  $> 50\sigma$  curves capture the incompleteness due to variable sensitivity as well as extended sources. The VCSS1 bright source catalog is  $> 50\%$  complete for sources with peak brightnesses above 200 mJy/bm or integrated fluxes above 300 mJy.

### 6.5. *Reliability*

Within the catalog were 53 sources not formally matched to sources in the literature. Visual examination revealed they are all components of resolved doubles and sources with complex structure. All are associated with cataloged sources at other frequencies. The reliability, defined as the fraction of sources that are real, of the VCSS1  $> 50\sigma$  catalog is 100%.

## 7. ACKNOWLEDGEMENTS

Basic research in Radio Astronomy at the U.S. Naval Research Laboratory is supported by 6.1 Base funding. Construction and installation of VLITE was supported by the NRL Sustainment Restoration and Maintenance fund. The National Radio Astronomy Observatory is a facility of the National Science Foundation operated under cooperative agreement by Associated Universities, Inc.

## REFERENCES

- Condon, J. J., Cotton, W. D., Greisen, E. W., et al. 1998, *AJ*, 115, 1693.  
doi:10.1086/300337
- Gaia Collaboration, Brown, A. G. A., Vallenari, A., et al. 2021, *A&A*, 649, A1. doi:10.1051/0004-6361/202039657
- Górski, K. M., Hivon, E., Banday, A. J et al. 2005, *ApJ*, 622, 759.  
doi:10.1086/427976
- Hale, C. L., McConnell, D., Thomson, A. J. M., et al. 2021, *PASA*, 38, 58.  
doi:10.1017/pasa.2021.47
- Hales, C. A., Murphy, T., Curran, J. R. et al. 2012, *MNRAS*, 425, 979.  
doi:10.1111/j.1365-2966.2012.21373.x
- Hopkins, A. M., Whiting, M. T., Seymour, N. et al. 2015, *PASA*, 32, 37.  
doi:10.1017/pasa.2015.37
- Intema, H. T., Jagannathan, P., Mooley, K. P., et al. 2017, *A&A*, 598, A78.  
doi:10.1051/0004-6361/201628536
- Lacy, M., Baum, S. A., Chandler, C. J., et al. 2020, *PASP*, 132, 035001.  
doi:10.1088/1538-3873/ab63eb
- Mohan, N. & Rafferty, D 2015, *Astrophysics Source Code Library*, ascl:1502.007
- Perley, R. A. & Butler, B. J. 2017, *ApJS*, 230, 7. doi:10.3847/1538-4365/aa6df9
- Rengelink, R. B., Tang, Y., de Bruyn, A. G. et al. 1997, *A&AS*, 124, 259.

## APPENDIX

## A. CATALOG DATA COLUMNS

Below we list the data columns given in the catalog. Note the flux errors are PyBDSF fitting uncertainties only and do not include the overall 15% VCSS1 flux reliability.

Name: VCSS source name

RA: source right ascension, in degrees

DEC: source declination, in degrees

E\_RA:  $1\sigma$  fitting error on the right ascension, in degrees

E\_DEC:  $1\sigma$  fitting error on the declination, in degrees

Total\_flux: fitted total, integrated Stokes I flux density of the source, in mJy

E\_Total\_flux:  $1\sigma$  fitting error on the total flux density, in mJy

Corrected\_Total\_flux: Total\_flux corrected for bias, in mJy

Peak\_flux: fitted peak Stokes I flux density per beam of the source, in mJy/beam

E\_Peak\_flux:  $1\sigma$  fitting error on the peak flux density per beam, in mJy/beam

Corrected\_Peak\_flux: Peak\_flux corrected for bias, in mJy/bm

Maj: FWHM of the source major axis, in arcsec

E\_Maj:  $1\sigma$  error on the FWHM of the major axis, in arcsec

Min: FWHM of the source minor axis, in arcsec

E\_Min:  $1\sigma$  error on the FWHM of the minor axis, in arcsec

PA: position angle of the source major axis measured east of north, in degrees

E\_PA:  $1\sigma$  error on the position angle of the major axis, in degrees

Isl\_Total\_flux: total, integrated Stokes I flux density of the island in which the source is located, in mJy. This value is calculated from the sum of all non-masked pixels in the island with values above three times the local rms

E\_Isl\_Total\_flux:  $1\sigma$  error on the total flux density of the island in which the source is located, in mJy

Isl\_rms: average background rms value of the island, in mJy/beam

Isl\_mean: average background mean value of the island, in mJy/beam

Resid\_Isl\_rms: average residual background rms value of the island, in mJy/beam

Resid\_Isl\_mean: average residual background mean value of the island, in mJy/beam

S\_Code: PyBDSF code defining source structure:

‘S’ = a single-Gaussian source that is the only source in the island

‘C’ = a single-Gaussian source in an island with other sources

‘M’ = a multi-Gaussian source

Compactness: Median source compactness metric from the VCSS snapshots catalog

SNR: source signal to noise ratio calculated as  $(\text{Peak\_flux} - \text{Isl\_mean})/\text{Isl\_rms}$